RSC Advances

PAPER

View Article Online
View Journal | View Issue

Cite this: *RSC Adv.*, 2021, **11**, 30156

A freeze–thaw PVA hydrogel loaded with guava leaf extract: physical and antibacterial properties†

William Xaveriano Waresindo, [ac] Halida Rahmi Luthfianti,[ac] Dhewa Edikresnha, [ac] Tri Suciati, [b] Fatimah Arofiati Noor [a] and Khairurrijal Khairurrijal *[ac]

A polyvinyl alcohol (PVA) hydrogel loaded with guava leaf extract (GLE) has potential applications as a wound dressing with good antibacterial activity. This study succeeded in fabricating a PVA hydrogel containing GLE using the freeze–thaw (FT) method. By varying the GLE concentration, we can adjust the physical properties of the hydrogel. The addition of GLE results in a decrease in cross-linking during gelation and an increase in the pore size of the hydrogels. The increase of the pore size made the swelling increase and the mechanical strength decrease. The weight loss of the hydrogel also increases because the phosphate buffer saline (PBS) dissolves the GLE. Increasing the GLE concentration caused the Fourier-transform infrared (FTIR) absorbance peaks to widen due to hydrogen bonds formed during the FT process. The crystalline phase was transformed into an amorphous phase in the PVA/GLE hydrogel based on the X-ray diffraction (XRD) spectra. The differential scanning calorimetry (DSC) characterization showed a significant decrease in the hydrogel weight over temperatures of 30–150 °C due to the evaporation of water from the hydrogel matrix. The zone of inhibition of the PVA/GLE hydrogel increased with antibacterial activity against *Staphylococcus aureus* of 17.93% per gram and 15.79% per gram against *Pseudomonas aeruginosa*.

Received 26th May 2021
Accepted 22nd August 2021

DOI: 10.1039/d1ra04092h

rsc.li/rsc-advances

Introduction

Guava plants (*Psidium guajava*) with a high bioactive content are widespread and thriving in Indonesia.[1] Guava plants have been widely used to cure fever, diarrhea, diabetes, hypertension, gingivitis, rheumatism, and inflammation. It has been shown that they also accelerate wound healing.[2] Guava leaves contain high levels of bioactive molecules, including terpenoids, tannins, steroids, flavonoids, saponins, and alkaloids.[3] Flavonoids are natural compounds with a polyphenolic structure consisting of two aromatic rings connected *via* a heterocyclic pyranic ring.[4] One derivative of flavonoids is quercetin (3,3′,4′,5,7-pentahydroxyflavone).[5] Quercetin has been shown to contain antioxidants, anti-inflammatory and neuroprotective, anti-cancer, antimicrobial, and anti-allergic compounds.[6–9] The quercetin content in guava leaf extract (GLE) is around 2.15–6.78% (w/w).[10,11]

The high quercetin content in GLE makes the guava plant a good choice for further development and application in medicine and the field of functional food. The current challenges are to find the correct encapsulation method, which is easy, low-cost, and has good performance. The encapsulation method of bioactive materials that is currently being developed is the hydrogel.

Hydrogels are polymers with a three-dimensional cross-linked structure containing hydrophilic groups capable of absorbing water.[12] Hydrogels can be made using natural polymers such as alginate, chitosan, gelatin, starch, gellan gum, and cellulose.[13–18] In addition, hydrogels manufactured using synthetic polymers such as polyvinyl alcohol (PVA), polyvinyl pyrrolidone (PVP), polyethylene glycol (PEG), and polyacrylic acid (PAA) have the advantage of better mechanical properties.[19–22] PVA is the polymer most widely used for hydrogels because it can produce hydrogels with good mechanical properties and is biocompatible.[23] PVA-based hydrogel has been successfully applied as a wound dressing, a drug delivery system, and tissue engineering.[24–26]

The use of hydrogels as wound coverings has been extensively studied since the skin, as the outer covering of the body, is the largest organ that protects internal organs and maintains normal body temperature.[27] If there is damage to the skin tissue due to an injury, the function of the skin will be impaired.

Wounds left untreated are vulnerable to infection by bacteria, which ultimately affects the wound healing process.[28] According to the World Health Organization (WHO), wound

[a]*Department of Physics, Faculty of Mathematics and Natural Sciences, Institut Teknologi Bandung, Jalan Ganesa 10, Bandung 40132, Indonesia. E-mail: krijal@fi.itb.ac.id*

[b]*Department of Pharmaceutics, School of Pharmacy, Institut Teknologi Bandung, Jalan Ganesa 10, Bandung 40132, Indonesia*

[c]*University Center of Excellence – Nutraceutical, Bioscience and Biotechnology Research Center, Institut Teknologi Bandung, Jalan Ganesa 10, Bandung 40132, Indonesia*

† Electronic supplementary information (ESI) available. See DOI: 10.1039/d1ra04092h

infection causes many deaths every year worldwide. This high mortality rate is caused by poor wound healing abilities and wound covers that cannot kill bacteria in the wound.[29] The ideal wound cover must have good mechanical properties (especially flexibility), be non-toxic and hypo-allergenic, absorb wound exudate, prevent bacterial infection, and maintain the necessary moisture around the damage for accelerated wound healing.[30]

Recently, several researchers have reported the synthesis of PVA hydrogels for wound dressing applications.[31–34] PVA has no natural antibacterial activity, so they have combined PVA with active ingredients that have antibacterial activity or have used a combination of natural polymers. Kumar *et al.* have combined PVA/chitosan with silver nanoparticles to obtain a hydrogel with excellent mechanical properties and promising antibacterial activity.[35] However, the scanning electron microscope (SEM) images showed small uniform porosity in this hydrogel due to the physical interaction between the PVA and the chitosan. In their research, Swaroop and Somashekarappa have reported a decrease in the degree of swelling of the PVA hydrogel with the addition of ZnO nanoparticles synthesized by gamma radiation.[36] Juby *et al.* have also previously succeeded in fabricating hydrogels with a mixture of silver nanoparticles, PVA, and gum acacia (polysaccharides) using gamma radiation.[37] The addition of acacia gum affected biocompatibility, decreased antibacterial activity against Gram-negative bacteria, and increased the degree of swelling of the hydrogel.

Hydrogel fabrication with gamma radiation has a greater cost and requires more complex equipment than the physical cross-linking method. For the application of wound dressings, a hydrogel fabrication with an easy and inexpensive physical cross-linking method is needed, which also has pores that can absorb wound exudates, good mechanical strength, and antibacterial activity that can inhibit the growth of Gram-positive and Gram-negative bacteria.

We have prepared PVA/guava leaf extract (GLE) hydrogels by varying the GLE concentration using the freeze–thaw (FT) method. The FT method can produce a non-toxic hydrogel because the synthesis process does not require a chemical cross-linking agent.[38] During the freezing process, the PVA polymer networks form intermolecular and intramolecular hydrogen bonds, as well as crystallites in which the PVA chains aggregate with ice crystals. The GLE in the PVA polymer network can affect the formation of crystallites, resulting in pores in the hydrogel structure. The presence of pores in the hydrogel structure, the high degree of swelling, and GLE, which has antibacterial activity, make the PVA/GLE hydrogel a good candidate for a wound dressing.

Experimental

Materials

Polyvinyl alcohol (PVA) with molecular weight in the range of 89 000–98 000 Da was purchased from Sigma-Aldrich, Singapore. Dried guava leaves were bought from Babah Kuya's local herbal store, Bandung, Indonesia. Deionized water and technical grade ethanol were purchased from Brataco Chemistry, Indonesia.

Guava leaf extraction

The extraction of guava leaves was carried out by the maceration method as described in our previous study.[39] The guava leaf powder (1000 g) was weighed out, then immersed in 10 L of technical grade ethanol. The macerated solution was collected and filtered once every day during this maceration process (three days). The collected macerate was then evaporated using a rotary evaporator to obtain guava leaf extract (GLE) paste. Based on this extraction method, we obtained 165.44 g of GLE paste. Furthermore, this paste was dried using the freeze-drying method at −50 °C for 24 h. Then the frozen paste was placed into a vacuum chamber at a temperature up to 38 °C in the pressure of 8 mBar for 24 h, so that sublimation occurred and the ice in the sample evaporated, producing completely dry GLE.

Preparation of the PVA/GLE hydrogel

The 10 wt% PVA solution was prepared by dissolving 10 g of PVA powder in 90 g of deionized water, then stirring it using a magnetic stirrer at 108 °C for 4 h until a homogeneous solution was obtained. The GLE solution was prepared at a concentration of 10 wt% with deionized water as a solvent, then stirred at 40 °C until it was homogeneous. The precursor solutions were then prepared with the ratios shown in Table 1.

The hybrid solutions prepared in this way were then put in the freezer at −25 °C for 20 hours (freeze) then stored at room temperature for four hours (thaw). For each sample, the FT process was repeated six times.

Hydrogel density

As density is a measurement of the mass per unit volume, hydrogel pieces were prepared and weighed and their dimensions were measured. The density (ρ) of hydrogel was determined by using

$$\rho = \frac{m}{V} \quad (1)$$

where m corresponds to the mass of the hydrogel (g) and V is the volume of the hydrogel (mL).

Hydrogel morphology

Morphological characterizations of the PVA/GLE hydrogels were performed using a scanning electron microscope (SEM) (JSM-6510LA, JEOL, USA). SEM microphotographs with

Table 1 Weight compositions of the hydrogel solutions

Sample	PVA/GLE weight ratio	PVA mass (g)	GLE mass (g)
PGL0	10 : 0	15	0
PGL1	10 : 1	15	1.5
PGL2	10 : 2	15	3
PGL3	10 : 3	15	4.5
PGL4	10 : 4	15	6
PGL5	10 : 5	15	7.5

magnifications of 200× and 1000× were used to observe pore size and cross-linking density of the hydrogels after freeze-drying.

Hydrogel pore size. High porosity is beneficial for the absorption of wound exudate and the transfer of nutrients and oxygen to the cells covered by the wound dressing.[40] Then, hydrogel pore size was determined by using ImageJ software (version 64-bit Java 1.8.0_172, NIH, USA).[41] Pore sizes of the hydrogels were obtained from SEM images with magnifications of 200×. The number of images analyzed from each hydrogel was 4 images in which each image had a size of 325 μm × 242.5 μm. By calibrating the ImageJ software using SEM images with known sizes, we determined the pore size and then plotted the pore size distribution of the hydrogel.

Degree of swelling

The maximum amount of liquid that can be absorbed and held by hydrogel is measured by the degree of swelling. This test uses a phosphate buffer saline (PBS) solution adjusted to the pH of the wound surface (7.4 for chronic wounds). The measurement of the degree of swelling was initiated by drying the hydrogel to a constant weight. Next, the sample was immersed in PBS at 37 °C and then it was weighed 0, 3, 6, 9, 12, 24, and 48 h after immersion. This test aims to investigate the absorption capacity of hydrogels for body fluids at various precursor compositions. The degree of swelling (SD) of hydrogel was obtained from[42]

$$\mathrm{SD} = \frac{m_i - m_0}{m_0} \times 100 \quad (2)$$

where m_0 represents the mass of the dry hydrogel and m_i is the mass of the swollen hydrogel at a specific time (gram).

Weight loss

Weight loss expresses the number of gel fractions remaining after the hydrogel was dissolved in PBS. The identification of weight loss was made by drying the hydrogel at a temperature of 50 °C to remove water content. Next, the hydrogel was immersed in a PBS solution with a pH of 7.4 for 48 h at 37 °C. The soaked hydrogel was dried again in the oven to determine the mass of the remaining gel. The amount of insoluble gel indicates the number of cross-links formed in the hydrogel. The weight loss (WL) was calculated using[43]

$$\mathrm{WL} = \frac{W_\mathrm{i} - W_\mathrm{d}}{W_\mathrm{d}} \times 100 \quad (3)$$

where the weight of the hydrogel after heating is W_i and the weight of the hydrogel after soaking in PBS and drying is W_d.

Fourier transform infrared (FTIR) spectroscopy

The functional group interactions of the hydrogel were characterized using FTIR spectroscopy (IRPrestige21, Shimadzu, Japan). The FTIR spectra of the hydrogel were collected to determine the structural changes that occur in the PVA hydrogel loaded with GLE. The wavenumber range used was 500–4000 cm^{-1} with the wavenumber resolution of 1.42 cm^{-1}. The transmittance data obtained from various samples were then analyzed to determine any bond structure changes.

X-ray diffraction (XRD) analysis

Crystallinity is one of the factors that significantly affect the mechanical properties of polymers. Hydrogel crystal phase identification was made using an X-ray diffractometer (PW 1700, Philips, USA). The X-ray source used Cu-K_α radiation at 40 kV and 40 mA; 2θ was from 10 to 70°.

Thermal properties

The thermal properties of the hydrogel are used to determine the state of the polymer and evaluate the interactions between the polymer molecules in the hydrogel.[44] The resulting differential scanning calorimetry (DSC) curves allow the determination of the melting temperature (T_m) and calculation of the degree of crystallinity (X_c) of hydrogel samples.[23] The thermal properties of the PVA powder, GLE powder, and PVA/GLE hydrogels were characterized using a differential scanning calorimetry (DSC) (STA PT1600, Linseis, USA). The measurement was carried out from 30 °C to 600 °C with a temperature increase rate of 10 °C min^{-1}. The degree of crystallinity (X_c) was obtained from [45]

$$X_\mathrm{c} = \frac{\Delta H_\mathrm{f}}{\Delta H_\mathrm{f}^0} \times 100 \quad (4)$$

where ΔH_f is the melting enthalpy and ΔH_f^0 refers to the melting enthalpy of a fully crystalline polymer (for PVA 138.60 J g^{-1}).[46]

Mechanical properties

The measurement method often used to determine the elasticity of hydrogels is the compression test.[47] The test is carried out by placing the hydrogel between two plates and compressing it. The pressure applied to the hydrogel surface and the change in the hydrogel compression distance are used to obtain a stress–strain curve.[48] The compression stress is the ratio of the compressive force to the hydrogel area. In contrast, the compression strain is the ratio of the change in the hydrogel's height when subjected to a compressive force.[49] The tool used was a Universal Tensile Machine (SM-200, Sinowon, China). Samples were prepared in blocks with dimensions of 20 mm × 5 mm × 3 mm. The compression modulus was determined by calculating the slope of the linear stress–strain fitting curve.[50] In addition, the compressive strength of the hydrogel was calculated using[49]

$$\mathrm{CS} = \frac{F}{A} \quad (5)$$

where F represents the compressive force (N) and A is the area of the compressed plane (m^2).

Antibacterial study

The PVA/GLE hydrogel antibacterial activity test was performed using the Kirby–Bauer (KB) test and the total plate count (TPC) method against *Staphylococcus aureus* (ATCC 6538) and *Pseudomonas aeruginosa* (ATCC 9027). Testing the PVA/GLE hydrogels using this method started with preparing a disc-shaped sample of the hydrogel with a diameter of 20 mm and

a thickness of 5 mm. Then the hydrogel was placed over Mueller–Hinton Agar (MHA) solid in a Petri dish. Each hydrogel sample was placed in a separate Petri dish and an inoculum of either *S. aureus* (1.3×10^6 CFU mL^{-1}) or *P. aeruginosa* (4.5×10^5 CFU mL^{-1}) was poured on top. The zone of inhibition was measured after 24 h of incubation at 37 °C.

A 10 μL aliquot was taken for each sample and diluted in a physiological sodium chloride solution several times to obtain a calculated bacterial concentration as described in our previous work.[51] One mL of diluted bacterial suspension was taken and rubbed evenly onto MHA in a Petri dish, then incubated for 24 h at 37 °C. After incubation, the bacterial colonies from the dilution were counted to determine the amount of bacterial-growth inhibition. The hydrogel antibacterial activity was determined by using[51]

$$\text{Anti bacterial activity} = \frac{[(\log \text{control}) - (\log \text{hydrogel})]}{(\text{mass}) \times (\log \text{control})} \quad (6)$$

The calculation of the number of normal colonies based on the Food & Drug Administration (FDA) standards is 25–250 colonies.[52]

Statistical analysis

The following experiments, *e.g.*, solution properties, hydrogel density, degree of swelling, weight loss, Young's modulus, and compressive strength were repeated three times. For the antibacterial study, the KB test and the TPC method were repeated three and two times, respectively. Specifically, for the TPC method, the number of samples for each variation in the composition of the PVA/GLE hydrogel was two ($n = 2$).

The results were expressed in mean ± standard deviation (SD). Statistical differences between groups were analyzed using one-way ANOVA followed by Tukey's HSD (honestly significant difference) post hoc test.[53] This statistical test employed the IBM SPSS 20 software (IBM, USA) to determine a significant difference with the confidence level higher than 95% ($p < 0.05$).[54]

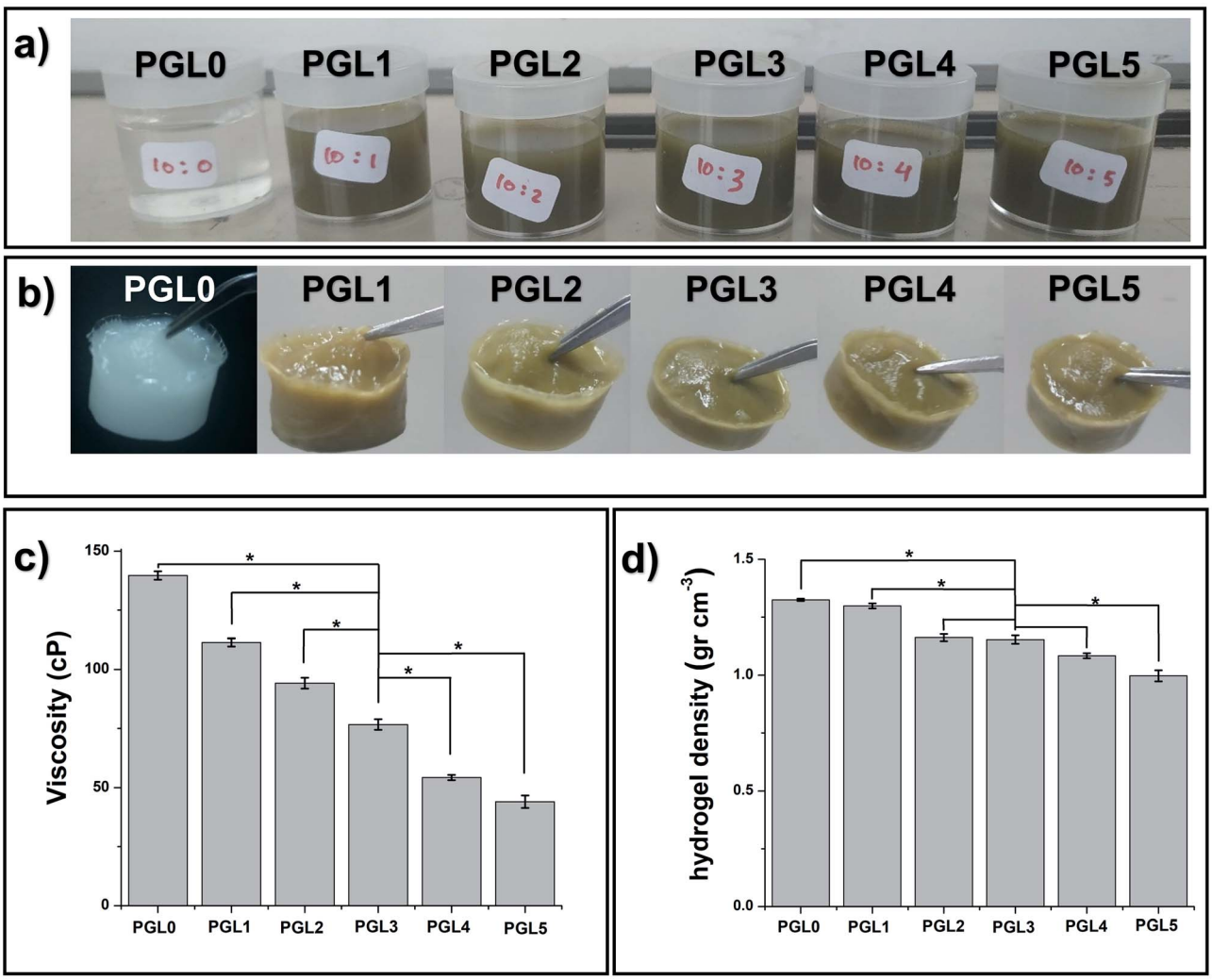

Fig. 1 (a) Precursor solutions with variation in GLE content, (b) hydrogel PVA/GLE produced by the FT method, (c) solution viscosity, and (d) the density of hydrogel. The values in (c) and (d) are expressed as mean ± SD of 3 samples ($n = 3$). The * sign indicates a significant difference between groups ($p < 0.05$).

Values with different superscript letters were significantly different ($p < 0.05$).

Results and discussion

Solution properties

The PGL0 solution, which is 10 wt% PVA, has distinctive physical characteristics: colourless, odourless, slightly sticky, and thick (Fig. 1a). Noting that the GLE solution is brownish-green and smelly, the addition of the GLE solution into the PVA solution caused the color of the PVA/GLE solution (which are the PGL1-PGL5 solutions) to become diluted.

Moreover, as shown in Fig. 1c, and Table 2, the viscosity, and the density of the PVA/GLE solution decreased because of more solvent contained in the GLE solution. The addition of the solvent made the ratio of the mass of the PVA to the total mass of the solution to decrease. The PGL0 solution had the viscosity and the density of 139.7 ± 1.8^{u} cP and 1.045 ± 0.013^{u} g cm^{-3}, respectively. These values reduced to be 44.0 ± 2.6^{z} cP and 1.028 ± 0.015^{u} g cm^{-3} for the PGL5 solution. There was a significant difference between groups ($p < 0.05$) in the solution viscosity due to the addition of GLE but the solution density showed no significant difference ($p > 0.05$).

Hydrogel density

The freeze–thaw (FT) method changed the sample from a solution to a gel, as shown in Fig. 1b. The FT method works through the formation of solvent molecule crystallites, which generates cross-linking and hydrogen bonding with water to form a hydrogel.

The measurement results depicted in Fig. 1d and listed in Table 2 showed a decrease in the hydrogel density due to changes in the internal structure of the hydrogel with the addition of the GLE.

The freezing stage results in the formation of hexagonal networks of hydrogen bonds with the water molecules present in the hydrogel network.[55] The one-way ANOVA test showed that there was a significant difference between groups ($p < 0.05$) in the hydrogel density. The PGL0 and PGL1 hydrogels significantly had the highest density compared to other groups. For the PGL2, PGL3, and PGL4 hydrogels, they have densities ranging from 1.08 to 1.16 g cm^{-3}. There was no significant difference between these groups ($p > 0.05$).

The PGL5 hydrogel (Fig. 1b and c) is more tenuous than the PGL0 hydrogel. Our initial assumption was that pores are formed, which will increase in size with GLE concentration. Furthermore, we investigated this assumption using an SEM.

Table 2 Solution properties and hydrogel density[a]

Sample	Viscosity (cP)	Solution density (g cm^{-3})	Hydrogel density (g cm^{-3})
PGL0	139.7 ± 1.8^{u}	1.045 ± 0.013^{u}	1.32 ± 0.05^{u}
PGL1	111.4 ± 1.7^{v}	1.043 ± 0.004^{u}	1.29 ± 0.02^{u}
PGL2	94.2 ± 2.3^{w}	1.041 ± 0.032^{u}	1.16 ± 0.05^{v}
PGL3	76.7 ± 2.2^{x}	1.036 ± 0.030^{u}	1.15 ± 0.01^{v}
PGL4	54.2 ± 1.1^{y}	1.029 ± 0.020^{u}	1.08 ± 0.01^{v}
PGL5	44.0 ± 2.6^{z}	1.028 ± 0.015^{u}	0.99 ± 0.02^{w}

[a] The values are expressed as mean ± SD of the 3 samples ($n = 3$). The use of superscripts on each column represent the statistical significant differences between groups. The groups with the same superscripts within each column indicate that the values are considered not significantly different ($p > 0.05$).

Hydrogel morphology

The morphological observations of the PVA/GLE freeze-dried hydrogels were intended to evaluate the hydrogel porosity distribution under dry conditions.[56] As shown in Fig. 2a, the pore size greatly affects the feasibility of the hydrogels for applications in the biomedical field. The PGL0 hydrogel (pure PVA hydrogel) shows a porous hydrogel morphology, which correlates with existing studies.[57,58]

In the PGL1, PGL2, PGL3, PGL4, and PGL5 hydrogels, when the GLE concentration was increased, it was seen that the pore sizes of the hydrogels had increased. Thangprasert *et al.* who investigated the effect of the addition of PVA concentrate on the resulting gelatin/PVA hydrogel morphology, concluded that a decrease in PVA concentration would cause an increase in the pore size.[26] The presence of PVA as a cross-linking agent decreases when GLE is added. Thus, in the present study, the sample PGL5 had the largest water content. When the hydrogel is freeze-dried, a sublimation process (ice crystal evaporation) occurs in the hydrogel and leaves a large pore.

Hydrogel pore size

The pore characteristics of hydrogels, such as pore structure, pore size, and porosity, can affect properties such as the absorbance capacity of water, swelling rate, mechanical strength, separation efficiency, and degree of sensitivity.[59] The optimal pore diameter for neovascularization (blood vessel) applications is 5 μm; for fibroblast growth, it is 5–15 μm; for skin regeneration of adult mammals, 20–125 μm; and for bone regeneration, 100–350 μm.[40]

The pore size distribution of each hydrogel given in Fig. 2b was non-linearly fitted to the Gaussian function using OriginPro 8.5.1 SR2 software (version 8.5.1 SR2, OriginLab Corporation, Northampton, MA, USA) to determine its average pore diameter. The results of pore size measurements in detail to see their distribution can be seen in Table S1†. In principle, the hydrogel pore size can be controlled by varying the freezing temperature in the freeze-drying process, resulting in hydrogel pores with a diameter of 1–250 μm.[60] In this study, however, the freeze-drying parameters used were kept constant. Therefore, the hydrogel pore size was only influenced by the variation of the precursor composition.

The average pore diameter of the PGL0 (pure PVA) hydrogel was 20.17 ± 5.62^{a} μm. On the other hand, Ceylan *et al.* synthesized PVA hydrogels using PVA with a molecular weight of 89 000–98 000 Da (in which the molecular weight was identical to that in the present study) using the FT method (freeze temperature of −16 °C for 20 h, thawing at room temperature for 3 h, and one FT cycle).[58] They obtained the average pore

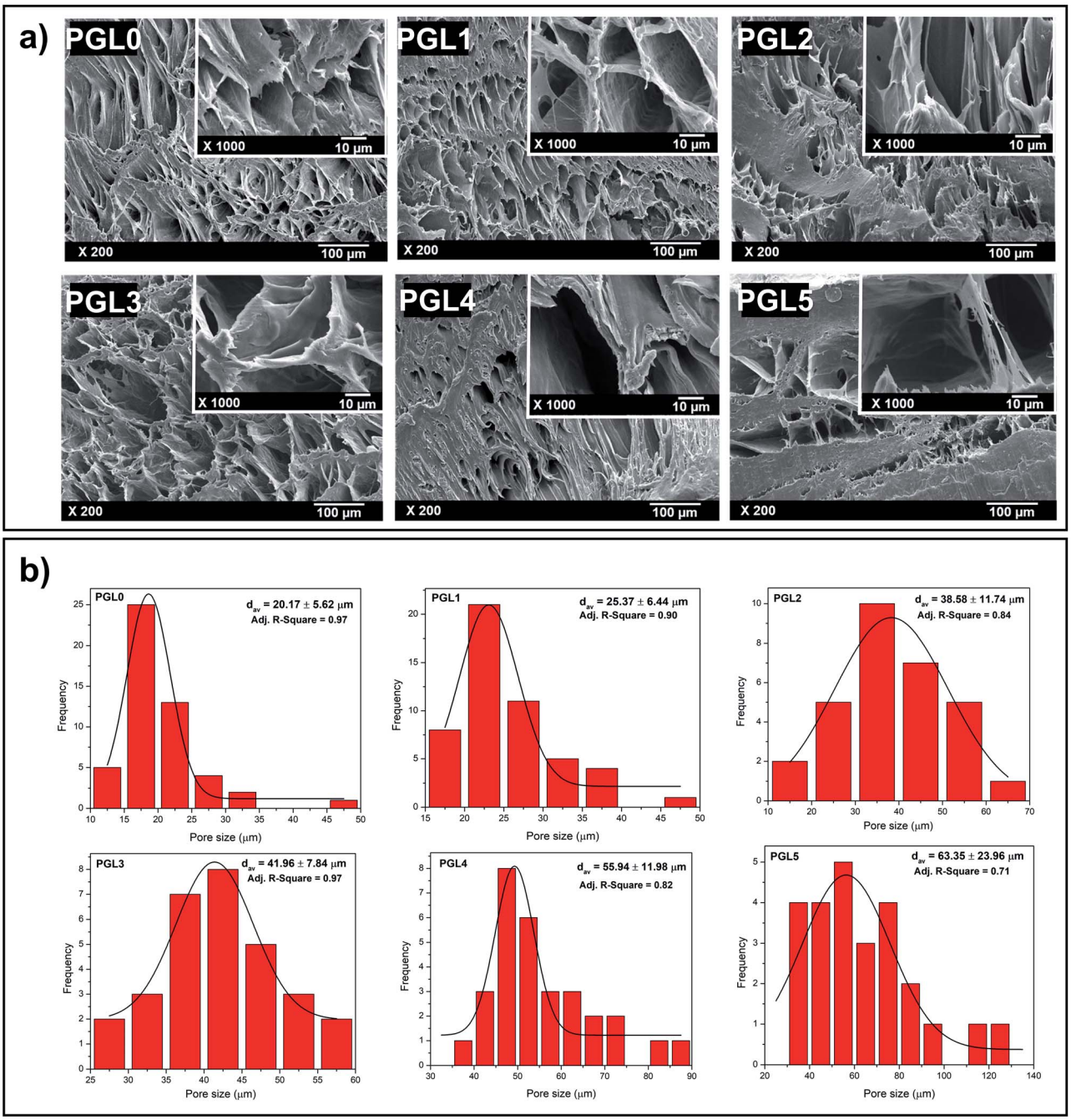

Fig. 2 (a) Morphologies of PVA/GLE hydrogels with different GLE concentrations (PGL0, PGL1, PGL2, PGL3, PGL4, and PGL5), (b) pore size distributions of PVA/GLE hydrogels based on non-linear curve fitting on OriginPro 8.5.1 SR2 software with the Gaussian as the peak function.

diameter of 3.69 μm, which is smaller than that of the PGL0. The reason is due to the differences in the freeze temperature and the number of FT cycles, resulting in different degrees of cross-linking and size of the ice crystals formed during the synthesis process.

The average pore diameters of the PGL0 and PGL1 hydrogels had no significant difference ($p > 0.05$). The statistical test is given in Table S2† also did not show a significant difference in the average pore diameter between PGL2 and PGL3, as well as between PGL4 and PGL5 ($p > 0.05$). Significant differences were obtained between the PGL0 and PGL1 hydrogels against the PGL2 and PGL3 hydrogels, and between the PGL4 and PGL5 hydrogels. Moreover, the average pore diameter increased with increasing GLE concentration for the PGL2, PGL3, PGL4, and PGL5 hydrogels. This addition caused a decrease in the PVA polymer content so that the degree of cross-linking decreased. The decrease in the degree of cross-linking resulted in a reduction of hydrogel density (Fig. 1d and Table 2) and an increase in

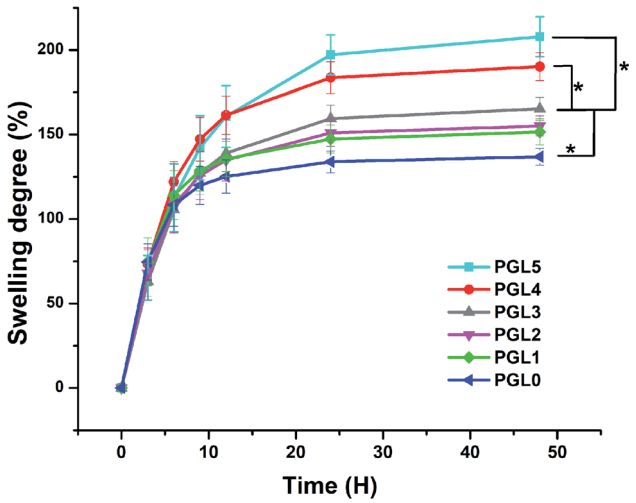

Fig. 3 Degree of swelling of PVA/GLE hydrogels in PBS solutions. Each point represents the average of the results from three different samples ($n = 3$). The * sign indicates a significant difference between groups ($p < 0.05$).

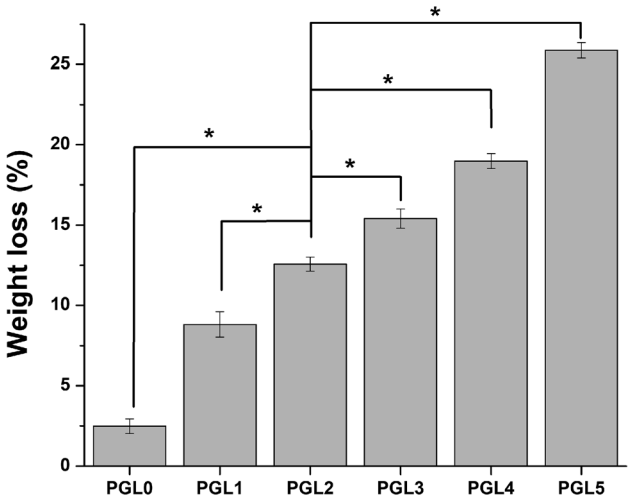

Fig. 4 Weight loss of PVA/GLE hydrogels after immersion in PBS for 48 hours. The values are expressed as mean ± SD of the 3 samples ($n = 3$). The * sign indicates a significant difference between groups ($p < 0.05$).

water content. The high-water content of the PGL5 hydrogel will leave large diameter pores (63.35 ± 23.96^{c} μm) when it is freeze dried.

Degree of swelling

The degree of swelling indicates the ability of the hydrogel to absorb water. It was found that the degree of swelling of the PVA/GLE hydrogels increased with increasing the GLE concentration, as demonstrated in Fig. 3.

All variations of the samples showed a significant increase from 0 to 12 hours. The expansion continued (but the increase was less significant) until the 24th hour, then reached a swollen equilibrium state.[61] The PGL0 hydrogel showed the lowest degree of swelling, around 135 ± 5^{a}% because it had the smallest pore size, and thus its ability to absorb PBS solution was also smaller than other hydrogels. This finding was confirmed by the previous study of Croitoru *et al.*[62]

The PGL1, PGL2, and PGL3 hydrogels had degrees of swelling that increased with the addition of GLE, namely $151 \pm 7^{a,b}$%, $155 \pm 5^{a,b}$%, and 165.3 ± 6.5^{b}%, respectively. The increase that occurred was not significant because the pore sizes of the PGL1, PGL2, and PGL3 hydrogels did not differ significantly ($p > 0.05$). The PGL4 hydrogel shows a degree of swelling around 189.3 ± 8.5^{c}% because it has an average pore diameter larger than those of the PGL0, PGL1, PGL2, and PGL3 hydrogels but smaller than that of the PGL5 hydrogel. The PGL5 hydrogel has the largest average pore diameter among the hydrogels. This allows the absorption of large amounts of PBS solution, up to 207 ± 12^{c}%.

Weight loss

The reduction in hydrogel weight expresses the number of parts of the hydrogel dissolved in PBS while measuring the degree of swelling, as shown in Fig. 4. Statistical tests on weight loss showed that there was a significant difference between groups ($p < 0.05$). The PGL0 hydrogel had a sturdier structure due to their higher cross-linked content. When immersed in PBS, the PGL0 hydrogel absorbed less liquid PBS than other hydrogels. The higher amount of cross-linking content causes the PGL0 hydrogel tend to retain its hydrogel structure. The weight loss of PGL0 was the smallest at 2.47 ± 0.46^{a}%.

The increase in GLE content in the PGL1, PGL2, PGL3, PGL4, and PGL5 hydrogels made the cross-linking content and the ability to maintain the hydrogel structure to decrease. The hydrogel dissolution process is characterized by a change in the PBS solution's colour from bright green to a more concentrated green. The PGL5 hydrogel showed the largest weight loss of 25.88 ± 0.48^{e}%, with a decreased sample size compared to the initial size before the process of measuring the degree of swelling.

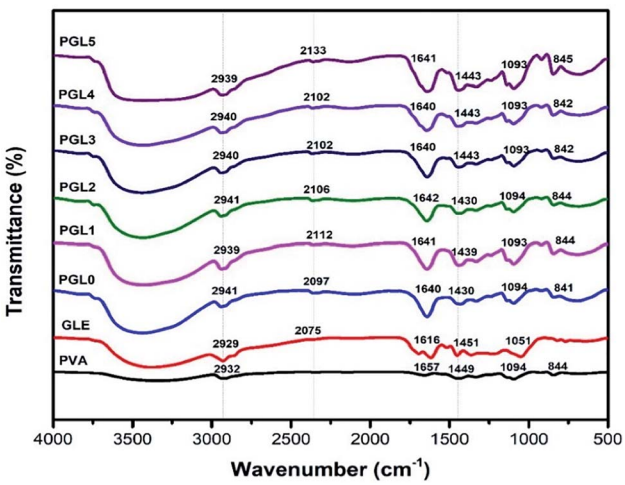

Fig. 5 FTIR spectra of the PVA powder, the GLE powder, and the PVA/GLE hydrogels with varied GLE contents.

Fourier transform infrared (FTIR) spectroscopy

The FTIR spectra of PVA powder (Fig. 5) showed absorbance peaks at 3200–3600 cm^{-1} (O–H stretch), 2932 cm^{-1} (C–H stretch), 1449 cm^{-1} (C–H bend), and 1094 cm^{-1} (C–O–C stretch). These results are consistent with previous study performed by Khorasani *et al.*[56] The 1094 cm^{-1} peak indicates a crystalline phase of PVA.[63]

The GLE has a broad absorbance peak due to the phenolic hydroxyl group (O–H stretch) at 3200–3600 cm^{-1}. The peaks at 2929 cm^{-1} shows the C–H stretch, at 2075 cm^{-1} due to the C–O stretch, and at 1616 cm^{-1} related to an aromatic ring of the carbonyl group (C=O). The peak at 1451 cm^{-1} confirms the C–H bending of the methyl groups', while the peak at 1051 cm^{-1} indicates the C–O–C stretch. These observations were also previously confirmed by Jeyasundari *et al.* and Rehan *et al.*[64,65]

The PGL0 hydrogel showed absorbance peaks similar to those of PVA powder. The difference is in the width of the peak of the hydroxyl group (stretching O–H). Sirousazar *et al.* indicated that the widening peaks of the hydroxyl groups of the PVA hydrogels could be caused by the crystallization of the PVA polymer chain and the formation of hydrogen bonds during the freeze–thaw process.[66] This also applies to the stretching of the C=O on the aromatic rings derived from the active ingredient of GLE. The addition of GLE causes the absorbance peak at the 1616 cm^{-1} to widen and the wavenumber to shift.

X-ray diffraction (XRD) analysis

The X-ray diffractograms obtained are presented in Fig. 6. The PVA powder showed a diffraction pattern with a sharp peak at an angle of $2\theta = 19.8°$ ($d = 4.58$ Å) related to the crystal plane orientation (101). Another diffraction peak is at $2\theta = 22.6°$ ($d = 3.93$ Å) related to the crystal plane orientation of (200). This diffraction pattern reveals that the PVA powder is crystalline, resulting from strong intermolecular interactions between the PVA chains due to the intermolecular hydrogen bonds.[67] The GLE powder only has one diffraction peak at $2\theta = 15.1°$ ($d = 5.3$ Å). In the range of $2\theta = 19°$–$50°$, the diffraction pattern was widened and had a greater slope (halo). This indicates that the GLE powder is semicrystalline and tends to become amorphous.[68]

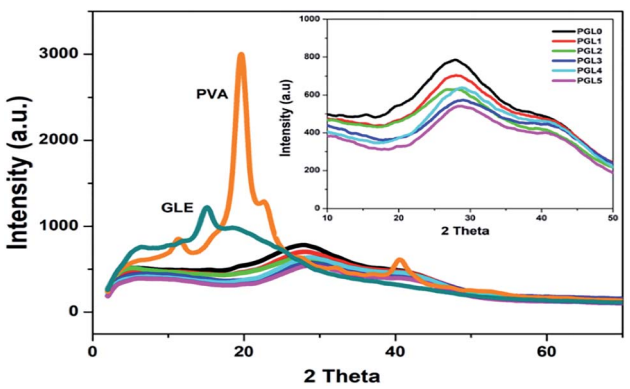

Fig. 6 XRD spectra of the PVA powder, the GLE powder, and the PVA/GLE hydrogels. The inset image shows that the diffraction peaks on the hydrogel widened with the addition of GLE concentrations for PGL0, PGL1, PGL2, PGL3, PGL4, and PGL5.

The PGL0, PGL1, PGL2, PGL3, PGL4, and PGL5 hydrogels showed a wide peak shift (halo) at an angular range of $2\theta = 26°$–$29°$, and there was a significant decrease in intensity as the GLE concentration was increased.

Specifically, the location of the halo peaks formed for each hydrogel is as follows: PGL0 at $2\theta = 26.9°$; PGL1 at $2\theta = 27°$; PGL2 at $2\theta = 26.7°$; PGL3 at $2\theta = 28.9°$; PGL4 at $2\theta = 29.1°$; and PGL5 at $2\theta = 29.1°$. The shift of the hydrogel peak towards the right, away from the PVA powder peaks at $2\theta = 19.8°$ and 22.6°, occurred due to increased water content and the decreased concentration of PVA. Thus the degree of crystallinity is also reduced.[69,70]

Thermal properties

The hydrogel decomposition due to thermal effects is demonstrated by the thermogravimetry-derivative thermogravimetry (TG-DTG) curves in Fig. 7a. The TG-DTG curves shows information about the decomposition phase, the maximum temperature of the DTG, and the residual weight percentage during the heating process at 600 °C. The weight losses in the temperature range of 30–150 °C, for PVA powder and GLE powder, were 6.21% and 7.73%, respectively. The highest percentage of residual weight at 600 °C was the GLE powder at 29.70%, followed by the PVA powder at 3.75%. The two precursors were dry and had less water content than the hydrogels. The GLE powder had the most significant percentage of residual weight at 600 °C because its thermal stability is achieved at higher temperatures, around 980 °C.[71]

The decomposition process of the hydrogel is divided into the evaporation phase of the water content and the decomposition of the solid hydrogel phase.[72] Evaporation of the water content in the hydrogel network starts at a 30 °C and continues to 150 °C. The evaporation process resulted in a weight loss of more than 80% for all hydrogels. The decomposition phase of the hydrogels that have lost their liquid components started at 155 °C and continued to 400 °C. The weight loss in this phase ranged from 9% to 11%, related to the degradation of the polyene structure of the PVA chain.[73] Consequently, the hydrogel with the highest PVA concentration, which is the PGL0 hydrogel, had a greater shrinkage, 11.30%, than the other hydrogels. The PVA decomposition process continued at temperatures from 400 °C to 600 °C. There is a break in the PVA polymer main chain, resulting in carbon residues at this stage.[73,74] The phase change in the PVA/GLE hydrogels can be observed in the differential thermal analysis (DTA) curves in Fig. 7b and c.

The DTA curves of the PVA powder and the GLE powder did not show endothermic peaks at temperatures below 150 °C, because these two precursors were dry, so there was no water evaporation process, unlike in the hydrogels. These DTA characterization results are corroborated by the previous TG-DTG results, which showed a minimum weight percentage reduction. The DTA curves of the hydrogels shows broad endothermic peaks at heating temperatures below 150 °C. The width of the

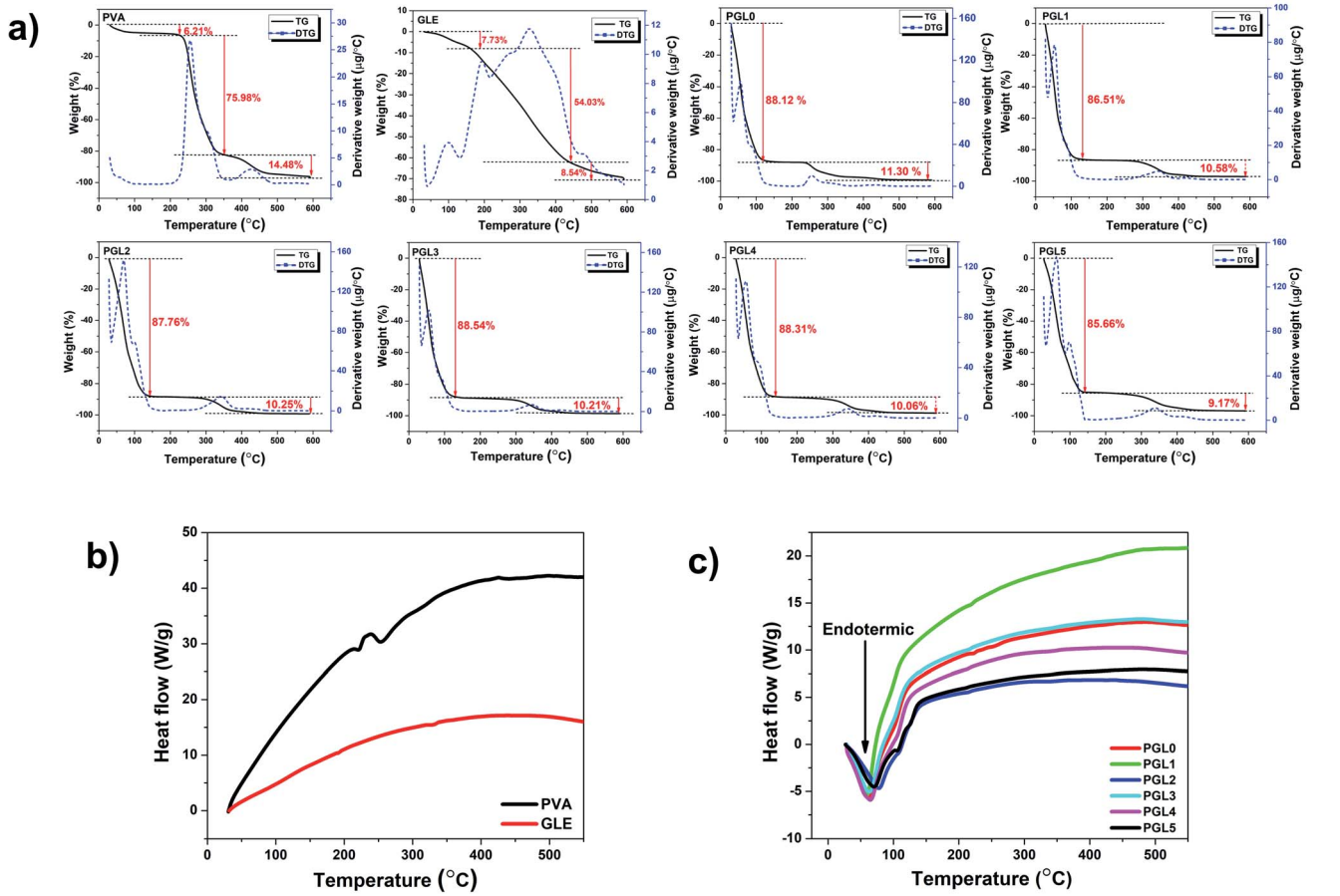

Fig. 7 (a)Thermal decomposition of the PVA powder, the GLE powder, and the PVA/GLE hydrogel at 30–600 °C, (b) DTA curves of the PVA and GLE powders, (c) DTA curves of the PVA/GLE hydrogel.

endothermic curve indicates a significant fusion of the sample. The melting in question is the evaporation of the water content of the hydrogel that has been confirmed in the TG-DTG curve. The DTA characterization can also be used to determine the melting temperature (T_m) of the sample, as shown in Table 3. We can determine the heat of fusion from the melting temperature value by calculating the area under the curve.[75]

The PVA powder starts to melt at 222 °C, while the GLE powder starts to melt at 192 °C. The melting points of the hydrogels from PGL0 to PGL5 decreased to lower temperatures (222 °C to 209 °C and 439 °C to 334 °C) due to the reduction in PVA concentration. Similar results were shown in the previous studies by S. Gupta *et al.*[76] Calculated area under the heat of fusion curve and degree of crystallinity are presented in Table 3.

The heat of fusion and degree of crystallinity of PVA had a significant difference ($p < 0.05$). The PVA powder has the largest heat of fusion of 44.80 ± 1.28^{t} J g^{-1}. The high value of the heat of fusion of the PVA powder caused the degree of

Table 3 Melting temperature, the heat of fusion, and the degree of crystallinity of PVA powder, GLE powder, and PVA/GLE hydrogel[a]

Sample	T_m (°C)	Δ_m (J g^{-1}) during PVA melting	Degree of crystallinity (%)
PVA	222; 253; 439	44.80 ± 1.28^{t}	32.31 ± 0.08^{t}
GLE	192; 325	—	—
PGL0	221; 250; 423	10.81 ± 0.85^{u}	7.80 ± 0.03^{u}
PGL1	218; 414	7.41 ± 0.56^{v}	5.34 ± 0.02^{v}
PGL2	214; 340	5.17 ± 0.64^{w}	3.73 ± 0.04^{w}
PGL3	213; 337	4.36 ± 0.38^{w}	3.14 ± 0.03^{x}
PGL4	211; 336	$3.52 \pm 0.35^{w,x}$	2.53 ± 0.05^{y}
PGL5	209; 334	1.78 ± 0.42^{x}	1.28 ± 0.03^{z}

[a] The value of heat of fusion, and degree of crystallinity was expressed as mean ± SD of 3 samples ($n = 3$). The use of superscripts on each column represent the statistical significant differences between groups. The groups with the same superscripts within each column indicate that the values are considered not significantly different ($p > 0.05$).

crystallinity to increase (32.31 ± 0.08^{t}%). The hydrogels showed a decrease in the heat of fusion and degree of crystallinity as they ranged from the PGL0 to PGL5 hydrogel. However, for the heat of fusion, there was no significant difference between groups of the PGL2, PGL3, and PGL4 hydrogels ($p > 0.05$). The reduced PVA content and increased GLE concentration in the PVA/GLE hydrogels were the leading causes of this downward trend. The PGL5 hydrogel had the lowest heat of fusion and the lowest degree of crystallinity at 1.78 ± 0.42^{x} J g^{-1} and 1.28 ± 0.03^{z}%, respectively.

Mechanical properties

The compression stress–strain curve in this study is depicted in Fig. 8. Wang *et al.* have presented the stress–strain curve of a PVA/carbon dots (CDs) composite hydrogel, which has a significant increase in stress values at strains of 30–85%.[77]

The stress–strain curves obtained in this study show similar characteristics, increasing stress values at the percentage strain of 50–95% for all samples. The curve of the PGL0 hydrogel has a sharper gradient than the other hydrogels. This result has also been confirmed in the previous study of Jayaramudu *et al.* when observing the effect of variations in the concentration of cellulose nanocrystals (CNCs) on the mechanical properties of PVA/CNC hydrogels.[78] The sharper gradient of the PGL0 hydrogel indicates a larger compression modulus. We observed the compression modulus values at the three strain levels given in Fig. 9.

A compression strain level of 0–49% indicates a tiny increase in the value of the compressive stress (the slope of the curve is very small), with the compression modulus ranges from 0.00224–0.00714 kPa. The best scenario is that the compressive force acting on the hydrogel is evenly distributed over each part of the hydrogel. The strain level of 50–69% shows an increase in the compression modulus because the stress–strain curve has a sharper gradient than for the 0–49% strain. At this stage, the compressive force exerted on the sample is not evenly distributed in each part of the hydrogel sample because there is a reduction in the area (the sample begins to crumble). As a result, the compressive stress value will experience a greater

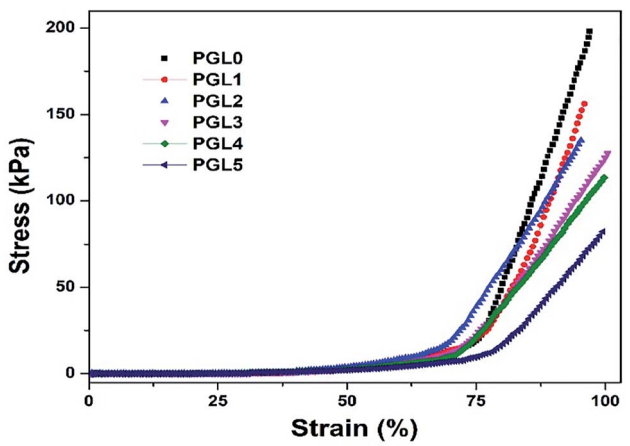

Fig. 8 Stress–strain curves of the PVA/GLE hydrogels.

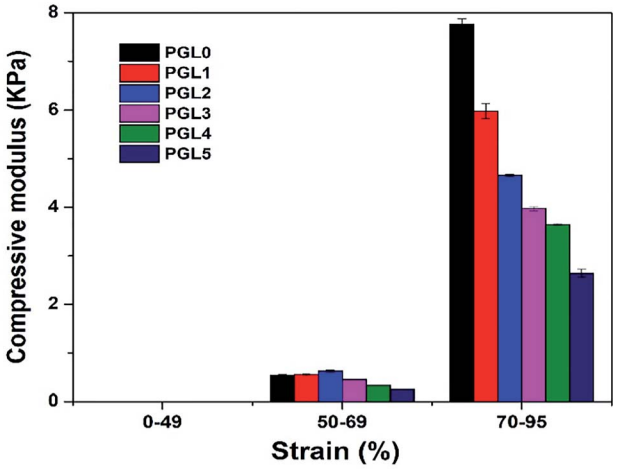

Fig. 9 The compressive modulus of the PVA/GLE hydrogels at strain levels of 0–49%, 50–69%, and 70–95%.

increase than the previous level and produce a sharper stress–strain curve. Compression modulus values at the 50–69% strain level ranged from 0.25–0.62 kPa.

The strain level of 70–95% is accompanied by a very significant increase in compression stress. A probable cause is the hydrogel sample experiencing massive destruction when the greater compressive force is used. The destruction of the sample results in a smaller contact area, resulting in an uneven distribution of the compressive force. Therefore, the value of the compression stress, which is inversely proportional to the compressed area, has increased. The modulus of compression based on a curve gradient showed values ranging from 2.64–7.76 kPa. According to Li *et al.* the compression modulus is highly dependent on the resulting strain ratio with an increase of up to 40 times the initial value.[49] In this study, we found that the increase in the modulus of elasticity reached 1000 times the initial value at a strain ratio of 0–95% and 15 times at 50–95% strain ratio. The variation in the composition of the PVA/GLE hydrogels affects the compressive modulus at each strain level, as given in Table 4.

There was no significant difference between groups of the PGL1, PGL2, PGL3, PGL4, and PGL5 hydrogels ($p > 0.05$) for the compression modulus at 0–50% strain ratio. However, the PGL0 hydrogel showed a significant difference with other groups for the same strain ratio ($p < 0.05$). The PGL0 hydrogel had a compression modulus of 0.52 kPa, which increased to 0.62 kPa in the PGL2 hydrogel, then gradually decreased to 0.25 kPa for the PGL5 hydrogel at a strain level of 50–69%. Similar results have been identified in previous studies by Wang *et al.* when they observed the effect of variations in the concentration of CDs on the compression modulus of PVA/CDs composite hydrogel.[77] When the variation of CDs had increased from 0% to 3%, the modulus of hydrogel compression increased from 0.4 kPa to 0.8 kPa, then began to decrease to 0.1 kPa when the CDs concentration was increased to 6%. At the strain level of 70–95%, an anomaly in the compression modulus is not observed as in the previous level. In this strain ratio, statistical tests

Table 4 Compressive moduli and compressive strengths of PVA/GLE hydrogels[a]

Sample	Compressive modulus at specified strain (kPa)			Compressive strength at 95% strain level (kPa)
	0–49%	50–69%	70–95%	
PGL0	0.0071 ± 0.0021^{u}	$0.52 \pm 0.02^{u,v}$	7.76 ± 0.11^{u}	208.47 ± 12.16^{u}
PGL1	0.0043 ± 0.0006^{v}	$0.55 \pm 0.02^{u,v}$	5.98 ± 0.16^{v}	184.65 ± 26.33^{u}
PGL2	0.0038 ± 0.0007^{v}	0.62 ± 0.02^{u}	4.65 ± 0.02^{w}	$162.25 \pm 35.90^{u,v}$
PGL3	0.0022 ± 0.0004^{v}	0.45 ± 0.01^{v}	3.96 ± 0.04^{x}	$129.97 \pm 3.38^{v,w}$
PGL4	0.0026 ± 0.0006^{v}	0.32 ± 0.06^{w}	3.64 ± 0.01^{y}	$114.50 \pm 5.17^{v,w}$
PGL5	0.0022 ± 0.0003^{v}	0.25 ± 0.06^{w}	2.64 ± 0.08^{z}	108.15 ± 0.73^{w}

[a] The value of compression modulus, and compressive strength were expressed as mean ± SD of 3 samples ($n = 3$). The use of superscripts on each column represent the statistical significant differences between groups. The groups with the same superscripts within each column indicate that the values are considered not significantly different ($p > 0.05$).

showed a significant difference between groups for all hydrogels ($p < 0.05$). The compression modulus of the PGL0 hydrogel, which is 7.76 ± 0.11^{u} kPa, decreases to 2.64 ± 0.08^{z} kPa for the PGL5 hydrogel. Jayaramudu *et al.* concluded that there was a decrease in the compression modulus of the PVA hydrogel with variations in the concentration of CNC.[78] They had investigated a pure PVA sample which showed a compression modulus value of 82 kPa and decreased with increased concentration of CNC (7%) to 7 kPa.

Human tissues, including skin, have Young's modulus values ranging from 1 to 100 kPa.[79,80] Based on the measurement results in this study, all samples at the 70–95% strain level met the application criteria as a wound dressing. They had a compression modulus value consistent with the range of Young's moduli of body tissues. Compressive strength is the ability to withstand induced loads to reduce size.[81] The stress–strain curve in Fig. 7a shows that all hydrogel samples have a curve resembling a "J," which indicates a high compressive strength in the hydrogel.[82]

According to Stauffer and Peppast, the compressive strength of the PVA hydrogel based on three freeze–thaw cycles, 10 hours of freezing, and one hour thawing, was 3.5 kPa.[83] The PGL0 hydrogel did not show a significant difference with the PGL1 and PGL2 hydrogels ($p > 0.05$) but did a significant difference to the other hydrogels ($p < 0.05$). In this study, we obtained a compressive strength of 208.47 ± 12.16^{u} kPa for the PGL0 hydrogel. This high compressive strength is influenced by the number of FT cycles: six cycles with a combination of FT time durations (20 hours to 4 hours). The addition of the number of cycles and a longer freeze duration can increase the cross-linked density resulting in a PVA hydrogel with better mechanical properties.[84]

The addition of GLE concentrate in the PGL1 to PGL5 hydrogels caused a very significant decrease in compressive strength values. However, the PGL3, PGL4, and PGL5 hydrogels had no significant differences between groups ($p > 0.05$).

The presence of GLE macromolecules and a reduction in the PVA concentration causes the cross-linked density to decrease.[85] This has previously been proven using SEM imaging, which shows an increase in pore size, and DTA characterization, which demonstrates a decrease in the degree of crystallinity of the hydrogel when the GLE concentration is increased.

Antibacterial study

The antibacterial properties of hydrogels are expressed by the zone of inhibition and the percentage of activity per mass unit.[86] An inhibition zone is created around the hydrogel during the incubation process due to the hydrogel sample's antibacterial activity, as presented in Fig. 10a. There was a significant difference between groups in the zone of inhibition both against *S. aureus* and *P. aeruginosa* ($p < 0.05$). Both *S. aureus* and *P. aeruginosa* were resistant to the PGL0 hydrogel, as evidenced by the absence of a clear zone around the sample. Based on previous research, PVA does not have antibacterial activity, so it cannot inhibit bacterial growth.[87]

The PGL1 hydrogel, which contains GLE, produces an inhibition zone of 14.93 ± 0.05^{a} mm for *S. aureus* and 13.94 ± 0.04^{a} mm for *P. aeruginosa*. Biswas *et al.* previously reported that the ethanol extract of guava leaves was able to form an inhibition zone of 11 mm against *S. aureus*.[88] Meanwhile, Hoque *et al.* obtained an inhibition zone for guava leaves extracted with ethanol of 15.3 mm against *S. aureus* and an inhibition zone for aqueous extract of guava leaves of 12 mm against *P. aeruginosa*.[89]

The ability of GLE to inhibit bacteria is influenced by the presence of polyphenol and flavonoid groups. These polyphenol and flavonoid groups can interact with bacterial cell membranes through hydrophobic–hydrophobic interactions, thereby increasing cell membrane leakage and damaging the structure of bacterial cells.[90] The inhibition zone formed against both types of bacteria was enlarged when the GLE concentration increased. Based on the classification of inhibition zone characteristics by Ouchari *et al.* the PGL1, PGL2, and PGL3 hydrogels (against *P. aeruginosa*) have "strong" inhibition zones (between 10–20 mm), whereas the PGL3, PGL4, and PGL5 hydrogels (against *S. aureus*) have "very strong" zones of inhibition (greater than 20 mm).[91] The inhibition zone diameter against *S. aureus* is greater than *P. aeruginosa* because of the difference in cell wall thickness of the two bacteria.[56] Furthermore, to determine the hydrogel antibacterial activity, we conducted tests using the total plate count method. The bacterial

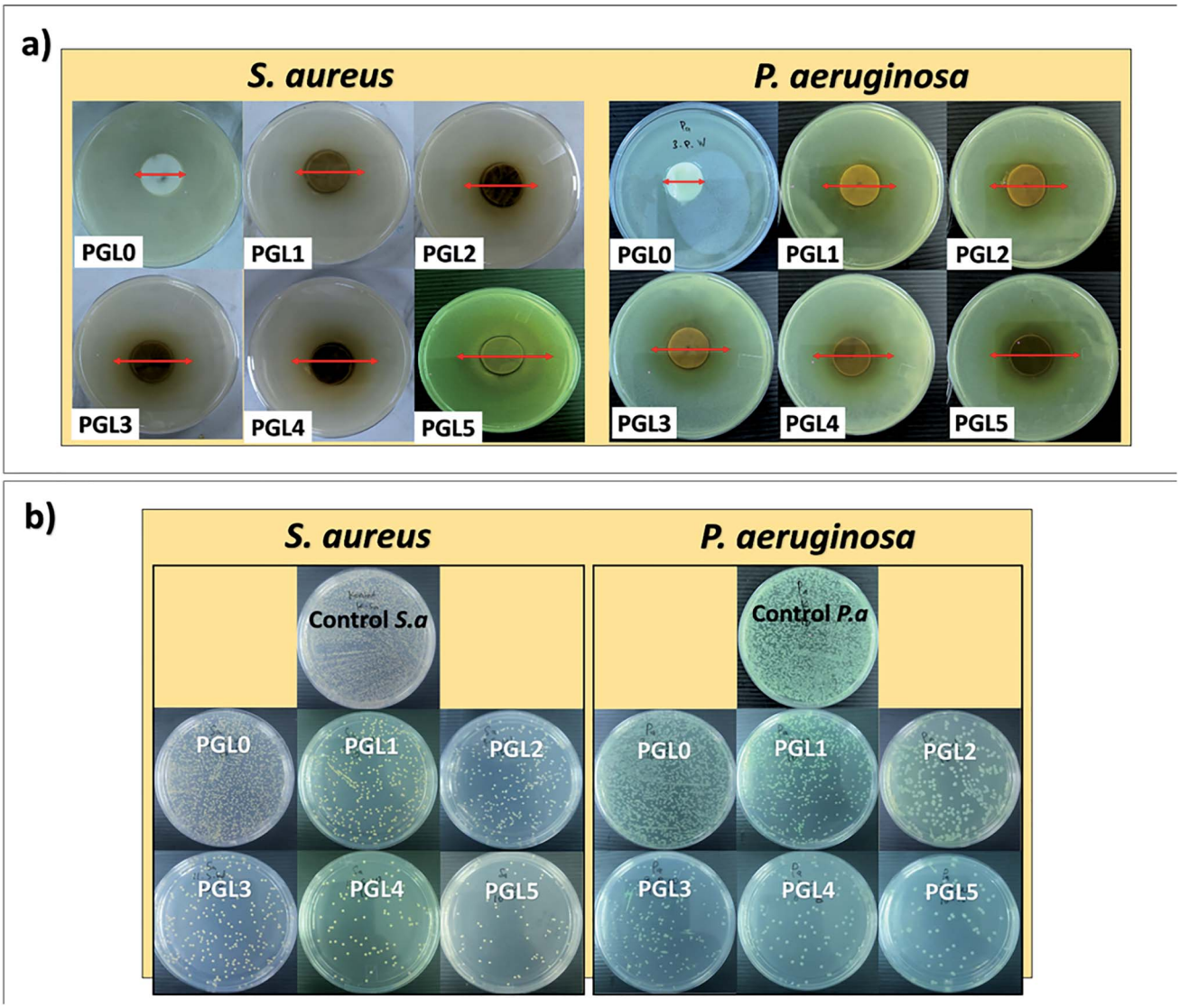

Fig. 10 (a) Zone of inhibition and (b) antibacterial activity of PVA/GLE hydrogels after 24 hours of incubation against *S. aureus* and *P. aeruginosa*.

suspension incubated for 24 hours at 37 °C will form a bacterial colony on MHA media, as shown in Fig. 10b. The best antibacterial activity can be seen in the number of bacterial colonies that are the least formed on the Petri dishes compared to the number of control colonies.[51] The number of *P. aeruginosa* bacteria was greater because of its smaller size with cell wall

Table 5 Zone of inhibition and antibacterial activity of PVA/GLE hydrogels after 24 hours incubation against *S. aureus* and *P. aeruginosa*

	Zone of inhibition (mm)		Weight (mg)		Log bacterial colonies after 24 h incubation (CFU mL^{-1})		Antibacterial activity of hydrogel (% per gram)	
Sample	*S. aureus*	*P. aeruginosa*	*S. aureus*	*P. aeruginosa*	*S. aureus*	*P. aeruginosa*	*S. aureus*	*P. aeruginos*[a]
PGL0	0	0	20.9	28.6	14.15	14.22	0.33 ± 0.02^{a}	0.19 ± 0.01^{a}
PGL1	14.93 ± 0.05^{a}	13.94 ± 0.04^{a}	23.9	29.1	10.88	13.04	9.85 ± 0.82^{b}	3.01 ± 0.04^{b}
PGL2	16.46 ± 0.10^{b}	15.42 ± 0.13^{b}	23.2	30.2	10.16	11.38	12.32 ± 0.65^{c}	6.73 ± 0.15^{c}
PGL3	20.31 ± 0.04^{c}	17.52 ± 0.06^{c}	22.8	28.5	9.07	8.28	15.92 ± 0.46^{d}	14.73 ± 0.47^{d}
PGL4	23.84 ± 0.06^{d}	23.32 ± 0.08^{d}	22.3	29.4	8.92	7.98	$16.70 \pm 0.55^{d,e}$	$15.01 \pm 0.63^{d,e}$
PGL5	34.55 ± 0.12^{e}	26.90 ± 0.15^{e}	21.2	29.0	8.80	7.74	17.93 ± 0.78^{e}	15.79 ± 0.29^{e}
Control	—	—	—	—	14.25	14.30	—	—

thicknesses ranging from 1.5–10 nm, while *S. aureus* had bacterial cell wall sizes ranging from 20–80 nm.[92] The calculation of antibacterial activity with eqn (6) is shown in Table 5.

Antibacterial activity against *S. aureus* showed significant differences between groups for the PGL0, PGL1, PGL2, and PGL3 hydrogels ($p < 0.05$). However, between the PGL 3 and PGL 4 hydrogels, and between the PGL4 and PGL5 hydrogels, there were no significant differences ($p < 0.05$). The PGL0 hydrogel had antibacterial activity of 0.33 ± 0.02^{a}% per gram and 0.19 ± 0.01^{a}% per gram against *S. aureus* and *P. aeruginosa*, respectively. The number of bacteria formed in PGL0 is almost as greater as the number in the control, indicating that PGL0 has a weak ability to fight bacteria. The PGL1 hydrogel gave the reduction in the number of bacterial colonies formed of 23.10% against *S. aureus* and 8.29% against *P. aeruginosa* compared to the PGL0. The presence of GLE inhibited the number of bacterial colonies formed, reaching 9.85 ± 0.82^{b}% per gram against *S. aureus* and 3.01 ± 0.04^{b}% per gram against *P. aeruginosa*. It appears that GLE is more effective in inhibiting the growth of *S. aureus* colonies than *P. aeruginosa* colonies. *P. aeruginosa* has an effective permeability barrier as a Gram-negative bacteria, consisting of a thin lipopolysaccharide exterior membrane called peptidoglycan, limiting the penetration of plant extrusions.[88] Peptidoglycan is a type of polysaccharide responsible for maintaining the integrity of the bacterial cell structure.[92] The additional GLE in the PGL2, PGL3, PGL4, and PGL5 hydrogels resulted in a reduction in the number of bacterial colonies. The smaller number of bacterial colonies formed indicates that the antibacterial activity of the PVA/GLE hydrogels is increasing. The PGL5 hydrogel contains the most GLE, allowing high hydrophobic interactions with bacterial cell membranes and damaging these cell structures for *S. aureus* and *P. aeruginosa*. The antibacterial activity of the PGL5 hydrogel was 17.93 ± 0.78^{e}% per gram against *S. aureus* and 15.79 ± 0.29^{e}% per gram against *P. aeruginosa*.

Practically, hydrogels that have antibacterial activity are needed for wound dressing applications, bone implant, dental infections, osteomyelitis, gastrointestinal infections, catheter infections, and prosthesis implant infections.[86] The practical applications mentioned above require a hydrogel with good antibacterial activity, in order to reduce the possibility of bacterial penetration into our bodies. Even though the bacteria had already entered, with the high ability to damage the bacterial membrane, the bacteria could not grow more because their growth had been inhibited by the antibacterial hydrogel which is very important to treat infections effectively.[93]

The PGL0 hydrogel has the highest PVA composition than the other hydrogels in the present study. The high PVA content allows the formation of more cross-links in the polymer chain during the gelation process. When there are more cross-links, the space around these cross-links will be smaller, this space is known as the mesh size, also known as the pore size of the hydrogel.[94] With decreasing PVA composition sequentially from the PGL1 to PGL5 hydrogel, the number of cross-links formed will also decrease and cause the pore size to increase. This pore size will further affect the antibacterial activity of the hydrogel. The porous morphology of the hydrogel allows the controlled release of antibacterial extract from the hydrogel matrix with different release profiles depending on the structure and pore size. Zou *et al.* stated that the hydrogel which has a large pore size and interconnected pores has excellent and long-term antibacterial activity against both *S. aureus* and *E. coli* bacteria.[95]

The large and interconnected pores can facilitate the rate of antibacterial release so that the antibacterial activity of the hydrogel is more effective. Antibacterial measurements using both the KB test and TPC method showed that the highest antibacterial activity was possessed by the hydrogels with the largest pore sizes (the PGL4 and PGL5 hydrogels). Furthermore, the hydrogels exhibiting homogeneous and interconnected pore sizes allow good nutrient exchange and cell migration for biomedical applications injected into the human body.[96]

The application of PVA in the biomedical field has been approved by the FDA due to its good biocompatibility and non-toxicity.[97] The PVA hydrogel has a high-water content, similar to the human tissue, and thus provide excellent biocompatibility.[98] The cytotoxicity test of PVA hydrogel was performed using the L929 mouse fibroblast cell culture. With a maximum PVA concentration at 10%, the IC_{80} value has been obtained and the cell viability will be reduced by 20% compared to the initial number of cultured cells. Therefore, PVA hydrogel can be applied as an extracellular matrix (ECM).[99]

PVA hydrogels can also be loaded with antibacterial components such as silver nanoparticles (AgNPs), chitosan, or gelatin.[37,100] The MTT test conducted by Rodríguez-Rodríguez *et al.* on HT29-MTX-E12 cells (a human colorectal adenocarcinoma) on PVA/chitosan/gelatin hydrogel showed that the cell viability percentage only decreased after incubation for 3 and 7 days but still had a value above 80%. Hence, it proved that the PVA/chitosan/gelatin hydrogel has a good biocompatibility and thus can be applied as a tissue engineering material.[100]

Regarding GLE, the biocompatibility has been demonstrated in many previous studies with the cytotoxicity tests included.[101–103] The cell viabilities of CCD-45 SK cells (human healthy skin fibroblasts) due to the presence of aqueous GLE and ethanolic GLE reached 63% and 93%, respectively. The percentage cell viability of HepG2 (human hepatocellular carcinoma cells) showed more promising results with a value of 50% or even lower. Based on the results, the GLE can thus be applied as a cytotoxic agent in medical treatment.[103] It was also found that the IC_{50} values in GLE ranged from 200 μg mL^{-1} to 250 μg mL^{-1} against Kasumi-1 leukaemia cells.[101,104] Thus, the cytotoxicity activity of GLE is very significant to inhibit the growth of these cancer cells. Therefore, the PVA hydrogels loaded with GLE could have good biocompatibility and cytotoxic activity.

Conclusions

We have successfully synthesized PVA/GLE hydrogels using the freeze–thaw method. Increasing the GLE concentration causes the pore size, degree of swelling, and weight loss to increase. FTIR analysis showed functional groups from the PVA powder and the GLE powder in the PVA/GLE hydrogel samples. According to XRD analysis, the increase in GLE content caused

the crystalline phase to become amorphous, and the degree of crystallinity decreased, based on the DSC analysis. The DTA interpretation showed a reduction in the melting temperature due to a decrease in PVA concentration. The decreasing concentration of PVA caused the density of the hydrogel cross-linking of the PVA and GLE to decrease so that the compressive modulus and compressive strength are lower. However, with increasing GLE, the inhibition zone against *S. aureus* and *P. aeruginosa* was more significant, and the antibacterial activity was higher.

Author contributions

W. X. W. worked on conceptualization, methodology, data curation and original drafting. H. R. L. oversees conceptualization, methodology, and data curation. D. E. and T. S. provide resources and carry out supervision. F. A. N. is responsible for resources, writing-reviewing and editing, and supervision. K. K. is responsible for resources, writing-review and editing, supervision, and funding acquisition.

Conflicts of interest

There are no conflicts to declare.

Acknowledgements

This research was financially supported by the Institute for Research and Community Service, ITB Research Grant in the fiscal years of 2020–2021 and Ristek-BRIN PTUPT Research Grant in the fiscal years of 2019–2020. We gratefully acknowledge the Indonesian Endowment Fund for Education (LPDP) for the provision of the master scholarships of W. X. W.

References

1 S. Susanto, M. Melati and S. A. Aziz, *Agrivita*, 2019, **41**, 48–54.
2 R. M. P. Gutiérrez, S. Mitchell and R. V. Solis, *J. Ethnopharmacol.*, 2008, **117**, 1–27.
3 A. Raj, V. Menon and N. Sharma, *Vegetos*, 2020, **33**, 750–758.
4 A. Ghorbani, R. Rashidi and R. Shafiee-Nick, *Biomed. Pharmacother.*, 2019, **111**, 947–957.
5 Y. Wang, B. Tao, Y. Wan, Y. Sun, L. Wang, J. Sun and C. Li, *Biomed. Pharmacother.*, 2020, **128**, 110372.
6 C. Caddeo, M. Gabriele, X. Fernàndez-Busquets, D. Valenti, A. M. Fadda, L. Pucci and M. Manconi, *Int. J. Pharm.*, 2019, **565**, 64–69.
7 S. M. Tang, X. T. Deng, J. Zhou, Q. P. Li, X. X. Ge and L. Miao, *Biomed. Pharmacother.*, 2020, **121**, 109604.
8 M. Güran, G. Şanlıtürk, N. R. Kerküklü, E. M. Altundağ and A. Süha Yalçın, *Eur. J. Pharmacol.*, 2019, **859**, 172486.
9 H. Ding, X. Liang, Q. Wang, M. Wang, Z. Li and G. Sun, *Carbohydr. Polym.*, 2020, **248**, 116797.
10 I. Batubara, H. Suparto and N. S. Wulandari, *IOP Conf. Ser. Earth Environ. Sci.*, 2017, **58**, 012060.
11 J. R. Hirudkar, K. M. Parmar, R. S. Prasad, S. K. Sinha, M. S. Jogi, P. R. Itankar and S. K. Prasad, *Microb. Pathog.*, 2020, **138**, 103807.
12 J. Cao, Y. Wang, C. He, Y. Kang and J. Zhou, *Carbohydr. Polym.*, 2020, **242**, 116420.
13 S. Homaeigohar, T. Y. Tsai, T. H. Young, H. J. Yang and Y. R. Ji, *Carbohydr. Polym.*, 2019, **224**, 115112.
14 V. Pawar, M. Dhanka and R. Srivastava, *Colloids Surf., B*, 2019, **173**, 776–787.
15 D. Lai, E. Li, Y. Yan, Y. Liu, J. Zhong, D. Lv, Y. Ke, H. Chen and T. Guo, *Org. Electron.*, 2019, **75**, 105409.
16 T. T. Koev, J. C. Muñoz-García, D. Iuga, Y. Z. Khimyak and F. J. Warren, *Carbohydr. Polym.*, 2020, **249**, 116834.
17 M. Das and T. K. Giri, *J. Drug Deliv. Sci. Technol.*, 2020, **56**, 101586.
18 S. Palantöken, K. Bethke, V. Zivanovic, G. Kalinka, J. Kneipp and K. Rademann, *J. Appl. Polym. Sci.*, 2020, **137**, 23–25.
19 W. Nafo and A. Al-Mayah, *Int. J. Non Lin. Mech.*, 2020, **124**, 103515.
20 A. Kuźmińska, B. A. Butruk-Raszeja, A. Stefanowska and T. Ciach, *Colloids Surf., B*, 2020, **192**, 4–9.
21 A. Brown, H. He, E. Trumper, J. Valdez, P. Hammond and L. G. Griffith, *Biomaterials*, 2020, **243**, 119921.
22 C. Shen, S. Tang and Q. Meng, *Colloids Surf., B*, 2019, **181**, 734–739.
23 P. A. Bersanetti, V. H. Escobar, R. F. Nogueira, F. dos S. Ortega, P. Schor and A. de A. Morandim-Giannetti, *Eur. Polym. J.*, 2019, **112**, 610–618.
24 H. Fang, J. Wang, L. Li, L. Xu, Y. Wu, Y. Wang, X. Fei, J. Tian and Y. Li, *Chem. Eng. J.*, 2019, **365**, 153–164.
25 M. Muchová, L. Münster, Z. Capáková, V. Mikulcová, I. Kuřitka and J. Vícha, *Mater. Sci. Eng. C*, 2020, **116**, 111242.
26 A. Thangprasert, C. Tansakul, N. Thuaksubun and J. Meesane, *Mater. Des.*, 2019, **183**, 108113.
27 N. Yadav, S. Parveen, S. Chakravarty and M. Banerjee, *Skin anatomy and morphology*, 2020.
28 L. I. F. Moura, A. M. A. Dias, E. Carvalho and H. C. de Sousa, *Acta Biomater.*, 2013, **9**, 7093–7114.
29 G. Tao, Y. Wang, R. Cai, H. Chang, K. Song, H. Zuo and P. Zhao, *Mater. Sci. Eng. C*, 2019, **101**, 341–351.
30 J. Boateng and O. Catanzano, *J. Pharm. Sci.*, 2015, **104**, 3653–3680.
31 F. He, H. Jiao, Y. Tian, L. Zhao, X. Liao, Z. Fan and B. Liu, *J. Biomater. Sci. Polym. Ed.*, 2018, **29**, 325–343.
32 J. Wang, C. Zhang, Y. Yang, A. Fan, R. Chi, J. Shi and X. Zhang, *Appl. Surf. Sci.*, 2019, **494**, 708–720.
33 T. Gao, M. Jiang, X. Liu, G. You, W. Wang, Z. Sun, A. Ma and J. Chen, *Polymers*, 2019, **11**, 11010171.
34 A. Shamloo, Z. Aghababaie, H. Afjoul, M. Jami, M. R. Bidgoli, M. Vossoughi, A. Ramazani and K. Kamyabhesari, *Int. J. Pharm.*, 2020, **592**, 120068.
35 A. Kumar, T. Behl and S. Chadha, *Int. J. Biol. Macromol.*, 2020, **149**, 1262–1274.
36 K. Swaroop and H. M. Somashekarappa, *Mater. Today: Proc.*, 2018, **5**, 21314–21321.
37 K. A. Juby, C. Dwivedi, M. Kumar, S. Kota, H. S. Misra and P. N. Bajaj, *Carbohydr. Polym.*, 2012, **89**, 906–913.

38 Y. Nagakawa, M. Kato, S. I. Suye and S. Fujita, *RSC Adv.*, 2020, **10**, 38045–38054.
39 Y. A. Rezeki, D. A. Hapidin, H. Rachmawati, M. M. Munir and K. Khairurrijal, *Adv. Powder Technol.*, 2020, **31**, 1811–1824.
40 N. Annabi, J. W. Nichol, X. Zhong, C. Ji, S. Koshy, A. Khademhosseini and F. Dehghani, *Tissue Eng., Part B*, 2010, **16**, 371–383.
41 C. A. Schneider, W. S. Rasband and K. W. Eliceiri, *Nat. Methods*, 2012, **9**, 671–675.
42 S. Bi, P. Wang, S. Hu, S. Li, J. Pang, Z. Zhou, G. Sun, L. Huang, X. Cheng, S. Xing and X. Chen, *Carbohydr. Polym.*, 2019, **224**, 115176.
43 J. Sittiwong, S. Niamlang, N. Paradee and A. Sirivat, *AAPS PharmSciTech*, 2012, **13**, 1407–1415.
44 Y. Guan, J. Bian, F. Peng, X. M. Zhang and R. C. Sun, *Carbohydr. Polym.*, 2014, **101**, 272–280.
45 S. Butylina, S. Geng and K. Oksman, *Eur. Polym. J.*, 2016, **81**, 386–396.
46 G. G. de Lima, B. D. Ferreira, M. Matos, B. L. Pereira, M. J. D. Nugent, F. A. Hansel and W. L. E. Magalhães, *Carbohydr. Polym.*, 2020, **245**, 116612.
47 C. T. Buckley, S. D. Thorpe, F. J. O'Brien, A. J. Robinson and D. J. Kelly, *J. Mech. Behav. Biomed. Mater.*, 2009, **2**, 512–521.
48 J. Xing, Y. Luo, J. Zhan and Z. Kang, *Int. J. Solids Struct.*, 2018, **144–145**, 301–312.
49 W. Li, D. Wang, W. Yang and Y. Song, *RSC Adv.*, 2016, **6**, 20166–20172.
50 D. Lee, H. Zhang and S. Ryu, *Cellul. Superabsorbent Hydrogels*, 2019, pp. 1–21.
51 D. Edikresnha, T. Suciati, M. M. Munir and K. Khairurrijal, *RSC Adv.*, 2019, **9**, 26351–26363.
52 A. Ben-David and C. E. Davidson, *J. Microbiol. Methods*, 2014, **107**, 214–221.
53 M. Bahadoran, A. Shamloo and Y. D. Nokoorani, *Sci. Rep.*, 2020, **10**, 7–9.
54 S. P. Lin, K. Y. Lo, T. N. Tseng, J. M. Liu, T. Y. Shih and K. C. Cheng, *Cell. Polym.*, 2019, **38**, 15–30.
55 J. Long, A. E. Etxeberria, C. Kornelsen, A. V Nand, S. Ray, C. R. Bunt and A. Seyfoddin, *ACS Appl. Bio Mater.*, 2019, **2**, 2766–2779.
56 M. T. Khorasani, A. Joorabloo, H. Adeli, Z. Mansoori-Moghadam and A. Moghaddam, *Carbohydr. Polym.*, 2019, **207**, 542–554.
57 M. G. Cascone, L. Lazzeri, E. Sparvoli, M. Scatena, L. P. Serino and S. Danti, *ACS Appl. Bio Mater.*, 2004, **15**, 1309–1313.
58 S. Ceylan, D. Göktürk and N. Bölgen, *Biomed. Mater. Eng.*, 2016, 27, pp. 327–340.
59 L. Xing, Z. Li, Q. Zhang, Y. Zhang, P. Liu and K. Zhang, *RSC Adv.*, 2018, **8**, 2622–2631.
60 X. Shen, J. L. Shamshina, P. Berton, G. Gurau and R. D. Rogers, *Green Chem.*, 2015, **18**, 53–75.
61 L. Münster, Z. Capáková, M. Fišera, I. Kuřitka and J. Vícha, *Carbohydr. Polym.*, 2019, **218**, 333–342.
62 C. Croitoru, M. A. Pop, T. Bedo, M. Cosnita, I. C. Roata and I. Hulka, *Polymers*, 2020, **12**, 560.
63 K. Ou, X. Dong, C. Qin, X. Ji and J. He, *Mater. Sci. Eng. C*, 2017, **77**, 1017–1026.
64 J. Jeyasundari, P. S. Praba, Y. B. A. Jacob, V. S. Vasantha and V. Shanmugaiah, *Chem. Sci. Rev. Lett.*, 2017, **6**, 1244–1252.
65 M. Rehan, O. A. Ahmed-Farid, S. R. Ibrahim, A. A. Hassan, A. M. Abdelrazek, N. I. M. Khafaga and T. A. Khattab, *ACS Sustainable Chem. Eng.*, 2019, **7**, 18612–18623.
66 M. Sirousazar and P. Khodamoradi, *Mater. Today Commun.*, 2020, **22**, 100719.
67 T. Liu, C. Jiao, X. Peng, Y. N. Chen, Y. Chen, C. He, R. Liu and H. Wang, *J. Mater. Chem. B*, 2018, **6**, 8105–8114.
68 C. Osorio, J. G. Carriazo and H. Barbosa, *Quim. Nova*, 2011, **34**, 636–640.
69 H. Pingan, J. Mengjun, Z. Yanyan and H. Ling, *RSC Adv.*, 2017, **7**, 2450–2459.
70 R. Ricciardi, F. Auriemma, C. Gaillet, C. De Rosa and F. Lauprêtre, *Macromolecules*, 2004, **37**, 9510–9516.
71 K. A. Athmaselvi, C. Kumar, M. Balasubramanian and I. Roy, *J. Food Process Eng.*, 2014, **2014**, 1–10.
72 F. Reguieg, L. Ricci, N. Bouyacoub, M. Belbachir and M. Bertoldo, *Polym. Bull.*, 2020, **77**, 929–948.
73 S. Sunaryono, A. Taufiq, N. Mufti, N. Hidayat, S. Rugmai, S. Soontaranon, E. G. R. Putra and D. Darminto, *IOP Conf. Ser. Mater. Sci. Eng.*, 2017, **202**, 012041.
74 M. Abasian, V. Hooshangi and P. N. Moghadam, *Iran. Polym. J.*, 2017, **26**, 313–322.
75 C. M. Hassan and N. A. Peppas, *Adv. Polym.*, 2000, **153**, 37–65.
76 S. Gupta, T. J. Webster and A. Sinha, *ACS Appl. Bio Mater.*, 2011, **22**, 1763–1772.
77 Y. Wang, Y. Xue, J. Wang, Y. Zhu, Y. Zhu, X. Zhang, J. Liao, X. Li, X. Wu, Y. X. Qin and W. Chen, *Polymers*, 2019, **11**, 11071112.
78 T. Jayaramudu, H. U. Ko, H. C. Kim, J. W. Kim, R. M. Muthoka and J. Kim, *Materials*, 2018, **11**, 1–11.
79 X. Tang, X. Gu, Y. Wang, X. Chen, J. Ling and Y. Yang, *RSC Adv.*, 2020, **10**, 17280–17287.
80 Y. Yu, H. Yuk, G. A. Parada, Y. Wu, X. Liu, C. S. Nabzdyk, K. Youcef-Toumi, J. Zang and X. Zhao, *Adv. Mater.*, 2019, **31**, 1–9.
81 D. Hadrys, T. Węgrzyn, J. Piwnik, L. Wszołek and D. Węgrzyn, *Arch. Metall. Mater.*, 2016, **61**, 123–126.
82 Y. Guan, X. M. Qi, B. Zhang, G. G. Chen, F. Peng and R. C. Sun, *Bioresources*, 2015, **10**, 1378–1393.
83 S. R. Stauffer and N. A. Peppast, 1992, **33**, 3932–3936.
84 T. H. Kim, D. B. An, S. H. Oh, M. K. Kang, H. H. Song and J. H. Lee, *Biomaterials*, 2015, **40**, 51–60.
85 M. D. Figueroa-Pizano, I. Vélaz, F. J. Peñas, P. Zavala-Rivera, A. J. Rosas-Durazo, A. D. Maldonado-Arce and M. E. Martínez-Barbosa, *Carbohydr. Polym.*, 2018, **195**, 476–485.
86 S. Li, S. Dong, W. Xu, S. Tu, L. Yan, C. Zhao, J. Ding and X. Chen, *Adv. Sci.*, 2018, **5**, 1700527.
87 A. Bernal-Ballen, J. Lopez-Garcia, M. A. Merchan-Merchan and M. Lehocky, *Molecules*, 2018, **23**, 3109.
88 B. Biswas, K. Rogers, F. McLaughlin, D. Daniels and A. Yadav, *Internet J. Microbiol.*, 2013, 746165.

89 M. D. Mahfuzul Hoque, M. L. Bari, Y. Inatsu, V. K. Juneja and S. Kawamoto, *Foodborne Pathog. Dis.*, 2007, **4**, 481–488.
90 O. O. Olatunde, S. Benjakul and K. Vongkamjan, *J. Food Biochem.*, 2018, **42**, 1–11.
91 L. Ouchari, A. Boukeskasse, B. Bouizgarne and Y. Ouhdouch, *Biol. Open*, 2018, 035410.
92 A. Mai-Prochnow, M. Clauson, J. Hong and A. B. Murphy, *Sci. Rep.*, 2016, **6**, 1–11.
93 K. Yang, Q. Han, B. Chen, Y. Zheng, K. Zhang, Q. Li and J. Wang, *Int. J. Nanomed.*, 2018, **13**, 2217–2263.
94 D. Perera, M. Medini, D. Seethamraju, R. Falkowski, K. White and R. M. Olabisi, *J. Microencapsul.*, 2018, **35**, 475–481.
95 S. Zou, Z. Wei, Y. Hu, Y. Deng, Z. Tong and C. Wang, *Polym. Chem.*, 2014, **5**, 4227–4234.
96 L. Pierau and D.-L. Versace, *Materials*, 2021, **14**, 787.
97 B. Cerroni, R. Cicconi, L. Oddo, M. Scimeca, R. Bonfiglio, R. Bernardini, G. Palmieri, F. Domenici, E. Bonanno, M. Mattei and others, *Heliyon*, 2018, **4**, e00770.
98 J. Li and D. J. Mooney, *Nat. Rev. Mater.*, 2016, **1**, 1–18.
99 L. Sankari, B. L. Fernandes, C. L. K. Rebelatto and P. R. S. Brofman, *Int. J. Polym. Mater. Polym. Biomater.*, 2020, **69**, 653–658.
100 R. Rodríguez-Rodríguez, C. Velasquillo-Martínez, P. Knauth, Z. López, M. Moreno-Valtierra, J. Bravo-Madrigal, I. Jiménez-Palomar, G. Luna-Bárcenas, H. Espinosa-Andrews and Z. Y. García-Carvajal, *J. Biomed. Mater. Res., Part A*, 2020, **108**, 81–93.
101 A. S. Levy and S. K. Carley, *Trop. J. Pharm. Res.*, 2012, **11**, 201–207.
102 W. C. Lee, R. Mahmud, R. Noordin, S. Pillai Piaru, S. Perumal and S. Ismail, *J. Essent. Oil-Bear. Plants*, 2013, **16**, 32–38.
103 G. A. Kemegne, N. Bettache, M. A. Nyegue, F.-X. Etoa and C. Menut, *Res. J. Pharm., Biol. Chem. Sci.*, 2020, **8**, 58–64.
104 K.-C. Chen, C.-L. Hsieh, C.-C. Peng, H.-M. Hsieh-Li, H.-S. Chiang, K.-D. Huang and R. Y. Peng, *Nutr. Canc.*, 2007, **58**, 93–106.